International Journal of Thermophysics, Vol. 28, No. 2, April 2007 (© 2007)
DOI: 10.1007/s10765-007-0170-6

Evaluation of Thermal Conductivity of Hyperstoichiometric UO_{2+x} by Molecular Dynamics Simulation

Sho Yamasaki,[1] Tatsumi Arima,[1,2] Kazuya Idemitsu,[1] and Yaohiro Inagaki[1]

The thermal conductivity of UO_{2+x} has been investigated by an equilibrium molecular dynamics (EMD) simulation up to 2000 K using the Born–Mayer–Huggins interatomic potential with the partially ionic model. In the present EMD system with the Green–Kubo method, the thermal conductivity was determined by the auto-correlation functions of energy and charge currents and the cross-coupling term. The thermal conductivity of UO_{2+x} decreased with an increase of x and temperature. Its temperature dependence was relatively small for large x values, which was attributed to phonon scattering by excess oxygens. In addition, the heat capacity was calculated using the phonon-level density deduced by the velocity auto-correlation function for constituent ions. The phonon velocity was also evaluated by the phonon-dispersion relationship. Using these thermal properties obtained by EMD calculations, the effect of excess oxygens on the phonon mean free path was discussed.

KEY WORDS: equilibrium molecular dynamics simulation; heat capacity; hyperstoichiometric uranium oxide; phonon mean free path; thermal conductivity.

1. INTRODUCTION

Uranium dioxide has been the most widely used nuclear fuel in light water reactors. In such fuels, oxygen atoms released by fission oxidize UO_2 with an increase in the burn-up and consequently raise the ratio of oxygen to

[1] Institute of Environmental Systems, Faculty of Engineering, Kyushu University, 744 Motooka, Fukuoka 812-8581, Japan.
[2] To whom correspondence should be addressed. E-mail: arimatne@mbox.nc.kyushu-u.ac.jp

uranium (O/M = 2 + x). In addition, the O/M ratio near the fuel center becomes larger than the nominal value since the temperature gradient is steeper in the fuel. In terms of the safety of the fuel management, the O/M ratio is one of the most important parameters because it significantly affects the thermal properties such as the melting point and thermal conductivity [1]. For example, the melting point decreases with an increase in the O/M ratio. However, the effect of the O/M ratio or x on such thermal properties has not been studied sufficiently, especially for $x > 0$ for which experimental difficulties are encountered. The oxygen stoichiometric parameter x is very sensitive to temperature, environment, impurities, etc. Unfortunately, a simulation study has not been carried out. Therefore, we focused on the thermal properties of hyperstoichiometric UO_{2+x} in the present simulation study.

Molecular dynamics (MD) simulations of UO_2 fuel have been successfully performed by several authors [2–6]. For stoichiometric UO_2, various thermal properties such as thermal expansion, ionic diffusion, specific heat, and thermal conductivity have been evaluated by equilibrium MD (EMD) calculations based on equilibrium thermodynamics. Although the thermal conductivity is a transport coefficient, it can be also calculated by the Green–Kubo relationship through the EMD simulation. Those studies have shown that the thermal conductivity of UO_2 decreases with increasing temperature, which results from the Umklapp process. For stoichiometric UO_2–PuO_2, EMD simulations have been performed [7,8]. These showed that the effect of Pu addition on the thermal conductivity was relatively small. Recently, we studied the hypostoichiometric $(U,Pu)O_{2-x}$ system by means of EMD simulation [9]. This previous study clearly showed that the thermal conductivity decreased with an increase in the oxygen deficiency x, which was caused by oxygen vacancies.

Therefore, in the present study, EMD simulations of hyperstoichiometric UO_{2+x} were performed to investigate thermal properties up to 2000 K, and the thermal conductivity was mainly studied in terms of the oxygen stoichiometric parameter x.

2. EQUILIBRIUM MOLECULAR DYNAMICS SIMULATION

In the present study, the MXDORTO program developed by Hirao and Kawamura [10] was used for the EMD simulations. This program is suitable for an orthogonal system. Here we employed the Born–Mayer–Huggins (BMH) potential with a partially ionic model (PIM) to each ion pair in simulated crystals. This potential function is given by

Table I. Born–Mayer–Huggins Interatomic Potential Parameters

Ion	z_i	a_i (nm)	b_i (nm)	c_i ($J^{-0.5}\cdot nm^3\cdot mol^{-0.5}$)	Source
U^{5+}	3.375	0.1201	0.00303	0.0	Present study
U^{4+}	2.70	0.1318	0.00360	0.0	[6]
O^{2-}	−1.35	0.1847	0.01660	1.294	[11,12]

$$U_{\mathrm{PIM}}(r_{ij}) = \frac{z_i z_j e^2}{r_{ij}} + f_0(b_i + b_j)\exp\left(\frac{a_i + a_j - r_{ij}}{b_i + b_j}\right) - \frac{c_i c_j}{r_{ij}^6}, \qquad (1)$$

where f_0 is an adjustable parameter. Potential parameters, a_i, b_i, and c_i, are associated with an ion of type i. The first term of the right side of Eq. (1) represents Coulomb interactions, which extend to long-range. In order to avoid divergence of the calculation related to the long-range term, an Ewald summation algorithm was introduced into the MD program. Other terms stand for short-range interactions: the second one is the repulsive potential between ionic cores, and the third one originates from van der Waals interactions. In Eq. (1), z_i is the effective charge of a type i ion, and an ionic bonding of 67.5% is assumed for each ion in the present simulated system. The ionicity and the potential parameters of the O^{2-} ion were obtained from the literature [11,12]. For the U^{4+} ion, the BMH potential parameters were determined in our previous study [6]. The potential parameters used in this study are summarized in Table I.

In order to discuss the thermal properties of hyperstoichiometric UO_{2+x}, the potential parameters of the U^{5+} ion are needed because the excess oxygen atoms result in the presence of such pentavalent uranium ions, U^{5+}, to maintain the electrical neutrality. In this case, hyperstoichiometric UO_{2+x} is described as $U^{4+}_{1-2x}U^{5+}_{2x}O^{2-}_{2+x}$. These excess oxygens might form the so-called 2:2:2 defect cluster, which was proposed by Willis [13,14]. The configuration of the 2:2:2 cluster is shown in Fig. 1. Here, we describe how to obtain the potential parameters of the U^{5+} ion. According to the U–O phase diagram [15], the UO_{2+x} phase with a fluorite structure ($Fm\bar{3}m$) exists from ~ 600 K to high temperature. Grønvold measured the lattice constant as a function of the O/M ratio for UO_{2+x} [16]. So we determined the potential parameters of U^{5+} ion based on the lattice constant from a MD fit of the experimental results for O/M ratios between 2.02 and 2.09 [16,17]. The result shown in Fig. 2 signifies an expansion of the lattice parameter with temperature, and its contraction is caused by excess oxygens.

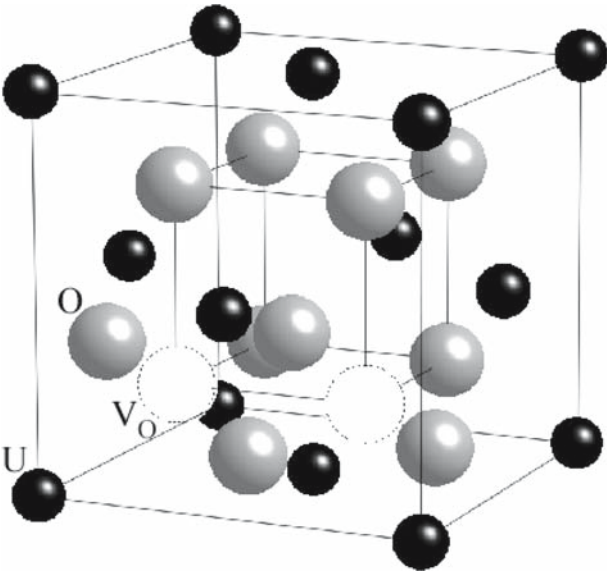

Fig. 1. Configuration of the 2:2:2 defect cluster in UO_{2+x} [13, 14]. U stands for uranium, O: oxygen, and V_O: oxygen vacancy.

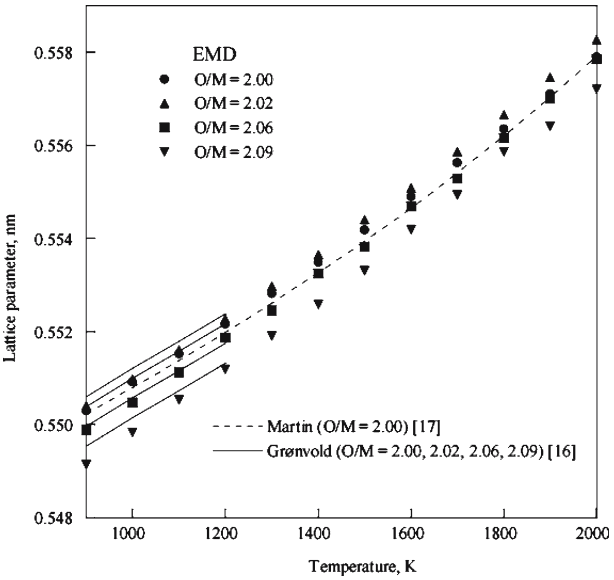

Fig. 2. Thermal expansion of UO_{2+x} as a function of temperature.

The EMD simulations were performed according to the following procedure. The U^{4+} and O^{2-} ions were arranged at each sub-lattice site of the fluorite structure composed of $3 \times 3 \times 3$ unit cells. For hyperstoichiometric UO_{2+x}, U^{5+} and excess O^{2-} ions were arranged like the configuration of the 2:2:2 cluster. Therefore, the simulated MD supercell consisted of a maximum of 334 ions for $UO_{2.09}$. In order to equilibrate the simulated system at the desired temperature and pressure, the so-called "initial relaxation" calculation was carried out for 2×10^4 steps (=40 ps). Then, the EMD simulation with 2×10^4 steps was performed in the *NPT* ensemble to determine the thermophysical properties other than the thermal conductivity. In order to obtain reliable results, calculations of the thermal conductivity were performed for a few runs of 5×10^5 time steps for one direction (x, y, or z) in the microcanonical ensemble (N,V,E).

3. RESULTS AND DISCUSSION

3.1. Thermal Conductivity of Hyperstoichiometric UO_{2+x}

In the present study, the thermal conductivity was calculated by the transport coefficients of the phenomenological equations composed of the charge current, energy current, and the cross-coupling term. The macroscopic charge and energy fluxes ($\vec{J}_Z$ and $\vec{J}_E$) are given by [3,18,19]

$$\vec{J}_Z = -L_{ZZ} T \nabla \left(\frac{\mu_Z}{T} \right) - L_{ZE} T \nabla (T), \tag{2}$$

$$\vec{J}_E = -L_{EZ} T^2 \nabla \left(\frac{\mu_Z}{T} \right) - L_{EE} \nabla (T). \tag{3}$$

In the above equations, $L_{\alpha\beta}$ ($\alpha, \beta = Z, E$) is the phenomenological coefficient and μ_Z is the electrochemical potential. The Onsager reciprocal relation gives $L_{ZE} = L_{EZ}$ so that the thermal conductivity can be expressed by

$$\kappa = L_{EE} - \frac{L_{EZ}^2}{L_{ZZ}} T. \tag{4}$$

According to the Green–Kubo relationship based on the fluctuation-dissipation theorem, such phenomenological coefficients, which relate to non-equilibrium phenomena, can be calculated under a thermal equilibrium condition. Therefore, in the EMD scheme, the phenomenological coefficients are given by the time integrals of the auto-correlation functions of microscopic fluxes, $\vec{j}_Z$ and $\vec{j}_E$;

$$L_{ZZ} = \frac{1}{3 V k_B T} \int_0^\infty dt \left\langle \vec{j}_Z(t) \cdot \vec{j}_Z(0) \right\rangle, \tag{5}$$

$$L_{EZ} = \frac{1}{3Vk_{\mathrm{B}}T^2} \int_0^\infty dt \left\langle \vec{j}_E(t) \cdot \vec{j}_Z(0) \right\rangle, \tag{6}$$

$$L_{EE} = \frac{1}{3Vk_{\mathrm{B}}T^2} \int_0^\infty dt \left\langle \vec{j}_E(t) \cdot \vec{j}_E(0) \right\rangle. \tag{7}$$

Here k_B is the Boltzmann constant and V is the cell volume for the simulation.

$$\vec{j}_Z(t) = \sum_{i=1}^{N} z_i e \vec{v}_i, \tag{8}$$

$$\vec{j}_E(t) = \sum_{i=1}^{N} \left[\frac{m_i v_i^2}{2} + \frac{1}{2} \sum_{j \neq i} U(r_{ij}) \right] \vec{v}_i + \frac{1}{2} \sum_{i=1}^{N} \vec{v}_i \cdot \vec{r}_{ij} \vec{F}_{ij}, \tag{9}$$

where m_i is the mass of the ith particle and v_i is its velocity. The last term, including the Coulomb potential in Eq. (9), is relatively complex compared to the Lennard-Jones potential [20–22]. This term has been already formalized for binary ionic systems, e.g., NaCl, KCl, CaF_2, UO_2, etc. by other researchers [3,4,19]. In the present study, in order to calculate the thermal conductivity, the algorithm proposed by Motoyama was incorporated into the MXDORTO program [4].

The transport coefficients and auto-correlation functions of energy given by Eq. (7) are plotted as a function of time in Fig. 3. The relaxation time becomes shorter at high temperatures for the same O/M ratio. This results from phonon scattering by the Umklapp process (three-phonon process) at high temperatures. At the same temperature, the relaxation time is decreasing for large O/M ratios. This is the reason that excess oxygens as lattice defects disorder the phonon conduction. Corresponding to the change of the relaxation time, the L_{EE} value decreases with increasing temperature and O/M ratio without the conditions of O/M = 2.09 and $T = 2000$ K. For a temperature of 2000 K, the other transport coefficients, L_{ZZ} and L_{EZ}, were calculated using Eqs. (5) and (6). Figure 4 shows that both transport coefficients are almost zero for O/M = 2.02. On the other hand, for O/M = 2.09, L_{EZ} is negative, which corresponds to a negative correlation between energy and charge fluxes. Simultaneously, a positive L_{ZZ} value shows that ionic conduction is occurring at high temperatures for large O/M ratios.

The thermal conductivity was calculated according to Eq. (4). For low temperatures and small O/M ratios, the thermal conductivity was the same as the transport coefficient L_{EE}. The results are shown in Fig. 5 as a function of temperature. In this figure, thermal conductivities obtained by experiments are also plotted [23–25]. The thermal conductivity of

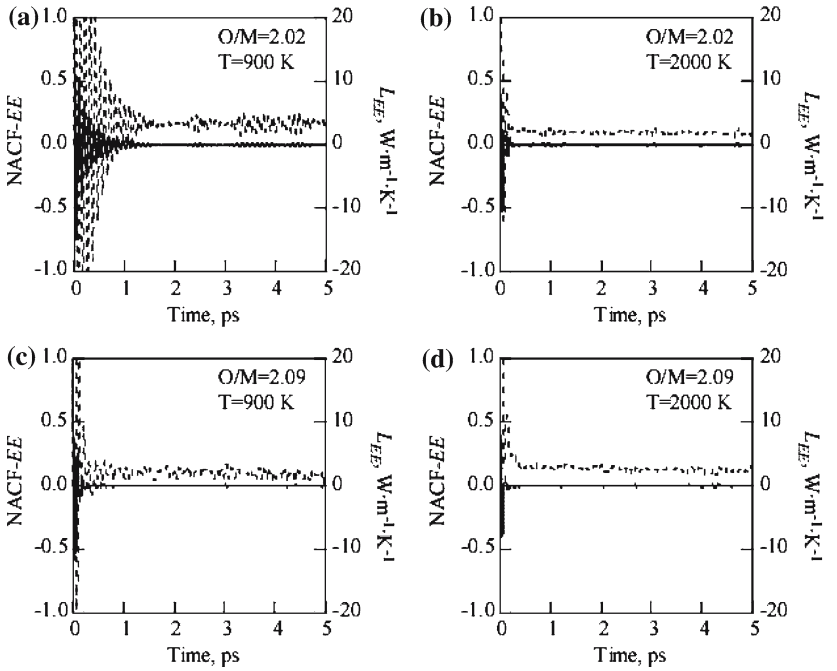

Fig. 3. Energy auto-correlation function NACF-*EE* and the energy transport coefficient L_{EE}.

UO_{2+x} decreases with increasing temperature and with oxygen stoichiometric parameter x. For such parameters, the results obtained by EMD calculations show a similar trend as experimental results, which explains the contributions from the Umklapp process and scattering by excess oxygens. For high temperatures, the experimental result increases slightly with temperature because of the contribution from the conduction electrons. On the other hand, in the EMD system, such a contribution was not considered. In addition, the magnetic contribution was neglected in EMD, and this effect was expected to be larger at low temperatures for $x = 0.0$ [26,27]. As a result, the thermal conductivity obtained for $x = 0.0$ by EMD might be a little larger than the present result. In terms of the simulation technique, EMD results seem to be somewhat scattered at high temperatures, but this disadvantage is expected to be overcome by the means of non-equilibrium MD [4].

3.2. Heat Capacity and Phonon Velocity Related to Thermal Conductivity

The heat capacity is an important thermal property along with the thermal conductivity. Using the present EMD simulation, the heat

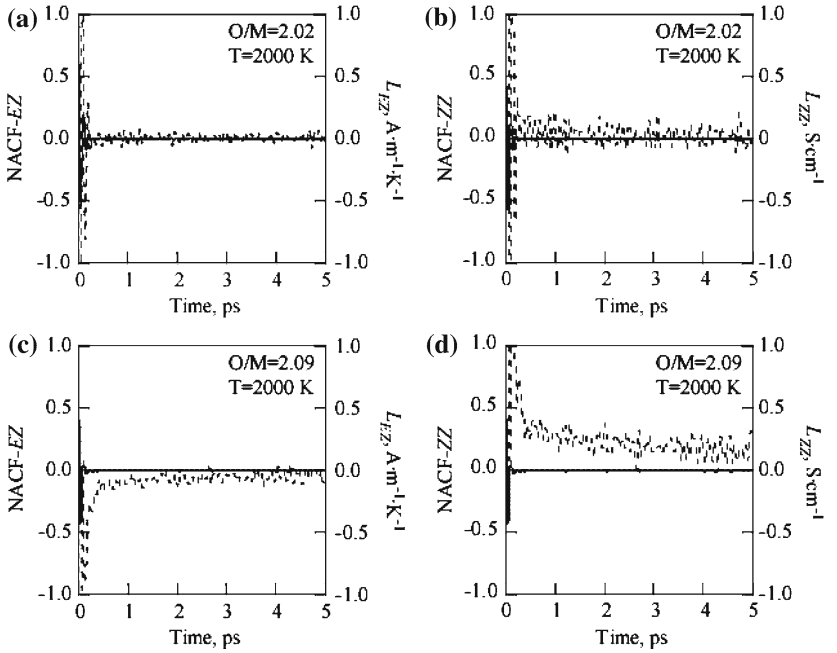

Fig. 4. Auto-correlation function between energy and ionic charge NACF-*EZ*, and the cross-coupling term L_{EZ}. NACF-*ZZ* and L_{ZZ} are the charge auto-correlation function and its integral (=the ion conductivity), respectively.

capacities (C_v and C_p) are calculated as follows [28]

$$C_{v,\mathrm{MD}} = \frac{3N}{k_\mathrm{B}} \int D(\omega) d\omega \left[\frac{\hbar\omega}{\exp(\hbar\omega / k_\mathrm{B} T)} \right]^2 \cdot \frac{\exp(\hbar\omega / k_\mathrm{B} T)}{T^2}, \tag{10}$$

$$C_{p,\mathrm{MD}} = C_{v,\mathrm{MD}} + 9\alpha^2 V_\mathrm{M} B_T T, \tag{11}$$

where $D(\omega)$ is the phonon-level density, α is the thermal expansion coefficient, V_M is the molar volume, and B_T is the bulk modulus. Here, the thermal expansion coefficient was obtained from Fig. 2, and the bulk modulus was estimated from the relationship between the MD supercell volume and pressure. The second term of the right side in Eq. (11) is called the dilation term, C_d. $D(\omega)$ is defined as the Fourier transform of the velocity auto-correlation function. The phonon-level density for each ion in UO_{2+x} at 900 K is shown in Fig. 6. The specific oscillation peak is smeared for O/M = 2.09, whereas they seem to be narrow for O/M = 2.00. The O ion has higher frequencies, which distributes over a wide range

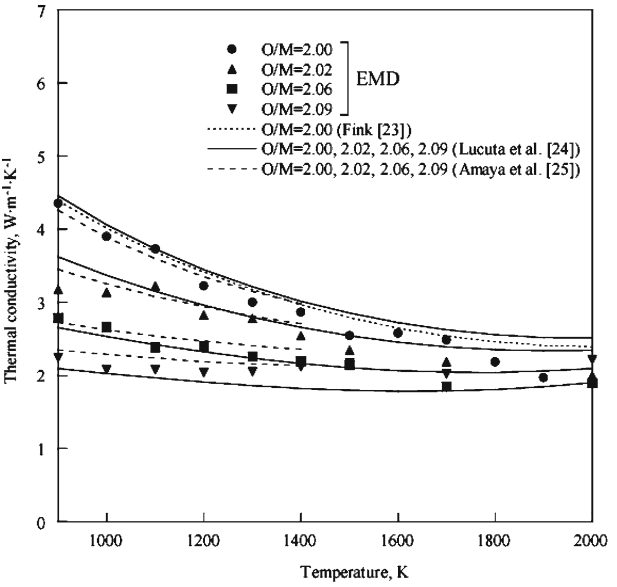

Fig. 5. Thermal conductivity of UO_{2+x} ($x = 0, 0.02, 0.06, 0.09$) as a function of temperature.

of frequency, in comparison with the U ion. In $UO_{2.09}$, the U ion has a valence of +4 or +5. As shown in Fig. 6c, for the U^{5+} ion, the peak strength seems to be a little larger at frequencies greater than ~6 THz. Thus, the heat capacities C_p of UO_{2+x} as shown in Fig. 7 are based on the phonon-level density and the dilation term. All terms in Eq. (11) were calculated by EMD. In Fig. 7, the heat capacity of UO_{2+x} increases with x. This is the reason why C_v increases with x, whereas C_d is almost insensitive to x. In order to compare with the results of EMD calculations, the recommended values in MATPRO are also plotted [29]. The difference between these results might originate mainly from the Schottky contribution, and above 1500 K, the contribution from the small polaron or the Frenkel defect is added. Such contributions were neglected in the EMD calculation.

In the present EMD system, the thermal conductivity was evaluated by either Eq. (4) or Eq. (7). Generally, the thermal conductivity is expressed by the following formula

$$\kappa = \frac{1}{3} C_v v_s l, \tag{12}$$

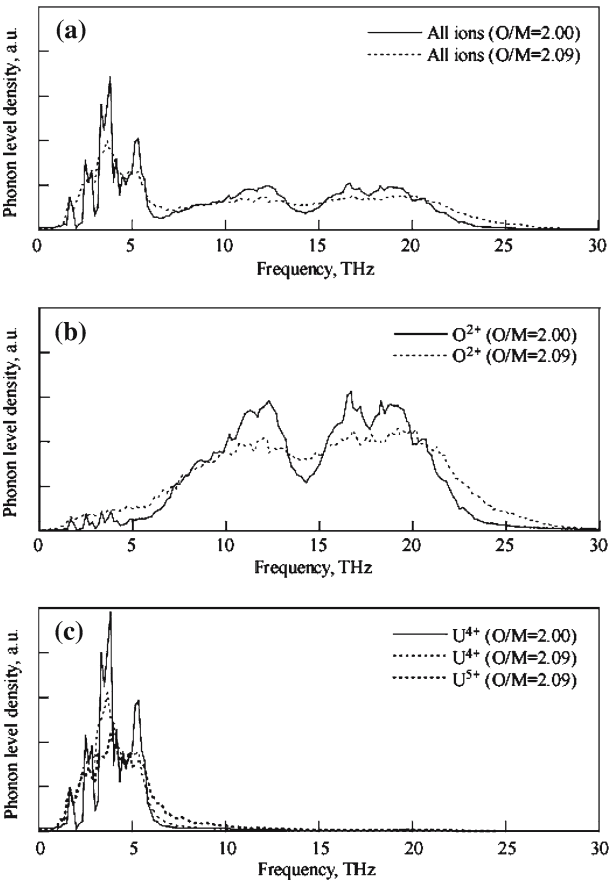

Fig. 6. Phonon-level density of UO_{2+x} $(x = 0, 0.09)$.

where v_s is the average phonon velocity $(=\sqrt{E/\rho}$; E is Young's modulus; ρ is the density), and l is the phonon mean free path. For the UO_{2+x} crystal, the phonon mean free path might be determined by the Umklapp process, by scattering by defects (or impurities), and by the magnetic moment of U, which can be expressed as $1/l = 1/l_{\mathrm{Umk}} + 1/l_{\mathrm{def}} + 1/l_{\mathrm{mag}}$. The last term l_{mag} was estimated to be ~ 5.1 nm for UO_2 and independent of temperature according to Moore et al. [27]. Of course, this term was missed in the EMD calculation. The values of C_v in Eq. (12) were obtained by the EMD calculation for UO_2 in our previous study. In order to evaluate the phonon velocity, the phonon-dispersion relationship, calculated for $[\zeta 00]$ by EMD, is shown in Fig. 8. The phonon velocity is

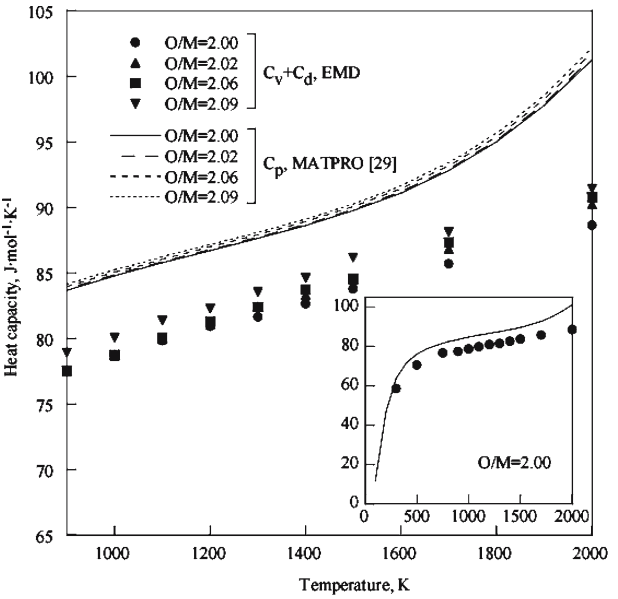

Fig. 7. Heat capacity of UO_{2+x} ($x = 0, 0.02, 0.06, 0.09$) as a function of temperature.

defined as the proportionality constant between the wave vector and frequency in their small regions. Both longitudinal and transverse phonon velocities, v_L and v_T, decrease slightly with increasing temperature and oxygen stoichiometric parameter x, but the variation is very small. For UO_2, v_L and v_T are obtained to be 6.1×10^3 and $3.0 \times 10^3 \mathrm{m \cdot s^{-1}}$, respectively, and Young's modulus was estimated to be 276 GPa based on these phonon velocities. As a result, the average phonon velocity is calculated to be $5.0 \times 10^3 \mathrm{m \cdot s^{-1}}$. On the other hand, the average phonon velocity was experimentally obtained to be $4.0 \times 10^3 \mathrm{m \cdot s^{-1}}$ [27]. If the phonon velocity is assumed to be $5.0 \times 10^3 \mathrm{m \cdot s^{-1}}$ in the EMD system, l_{Umk} is found to be 3.8 nm at 300 K and 0.79 nm at 1000 K for UO_2 using Eq. (12) and κ_{MD}. Consequently, l_{def} is found to be 0.86 nm for $UO_{2.09}$, and this value is comparable with l_{Umk} at 1000 K.

4. CONCLUSIONS

For hyperstoichiometric UO_{2+x}, EMD simulations were performed using the BMH potential with PIM in order to evaluate the thermal

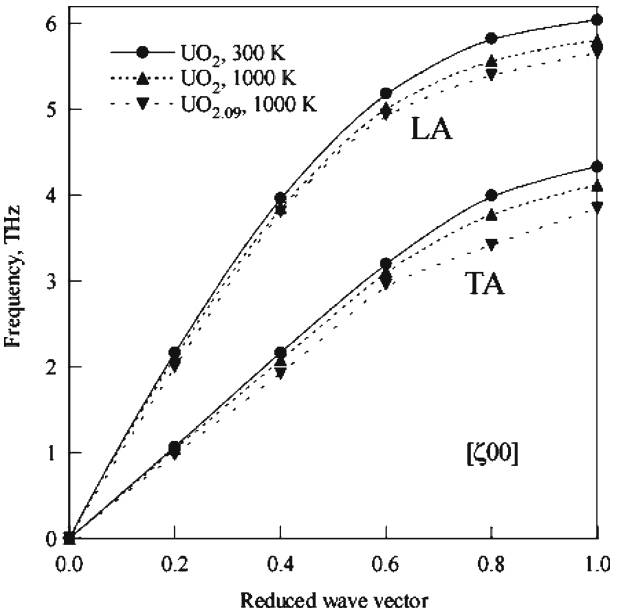

Fig. 8. Phonon-dispersion relationship of UO_{2+x} in the direction [ζ00]. LA stands for the longitudinal acoustic mode, and TA designates the transverse acoustic mode.

conductivity. In the present EMD system, the thermal conductivity was formulated by the transport coefficients in the phenomenological equations, which corresponded with the integrals of the auto-correlation functions given by the energy current, the charge current, and the cross-coupling term. The thermal conductivity for $x > 0$ was much smaller than that for $x = 0$ at low temperatures, and it decreased with temperature except for large values of x. The former was influenced by phonon disordering by the excess oxygens, and the latter originated from the Umklapp process (three-phonon process). Compared with experimental thermal conductivities, the present EMD simulation represents the stoichiometric parameter x and the temperature dependences of the thermal conductivity without the contribution due to scattering by the magnetic moment of U. The EMD results also showed that the heat capacity increased with x, whereas the phonon velocity was rather insensitive to x and temperature. According to the formula $\kappa = 1/3 C_v v_s l$, the phonon mean free path l was evaluated by the EMD calculations. Therefore, the mean free path due to scattering by excess oxygens was almost comparable to that due to the Umklapp process for $x = 2.09$ at 1000 K.

ACKNOWLEDGMENTS

The authors would like to thank K. Kawamura for usage of the MXDORTO program, and S. Motoyama for advice to calculate the thermal conductivity.

REFERENCES

1. D. R. Olander, *Fundamental Aspect of Nuclear Reactor Fuel Elements*, TID-26711-P1 (1976).
2. P. Sindzingre and M. J. Gillan, *J. Phys. C: Solid State Phys*. **21**:4017 (1988).
3. P. L. D. Lindan and M. J. Gillan, *J. Phys.: Condens. Matter*. **3**:3929 (1991).
4. S. Motoyama, Y. Ichikawa, Y. Hiwatari, and A. Oe, *Phys. Rev*. **B 60**:292 (1999).
5. K. Yamada, K. Kurosaki, M. Uno, and S. Yamanaka, *J. Alloys. Comp*. **307**:10 (2000).
6. T. Arima, S. Yamasaki, Y. Inagaki, and K. Idemitsu, *J. Alloys and Comp*. **400**:43 (2005).
7. K. Yamada, K. Kurosaki, M. Uno, and S. Yamanaka, *J. Alloys. Comp*. **307**:1 (2000).
8. K. Kurosaki, K. Yamada, M. Uno, S. Yamanaka, K. Yamamoto, and T. Namekawa, *J. Nucl. Mater*. **294**:160 (2001).
9. T. Arima, S. Yamasaki, Y. Inagaki, and K. Idemitsu, *J. Alloys Comp.* **415**:43 (2006).
10. K. Hirao and K. Kawamura, *Material Design Using Personal Computer* (Shokabo, Tokyo, 1994).
11. H. Inaba, R. Sagawa, H. Hayashi, and K. Kawamura, *Solid State Ionics*. **122**:95 (1999).
12. H. Hayashi, R. Sagawa, H. Inaba, and K. Kawamura, *Solid State Ionics*. **131**:281 (2000).
13. B. T. M. Willis, *Nature*. **197**:755 (1963).
14. B. T. M. Willis, *J. Phys*. **25**:431 (1964).
15. E. H. P. Cordfunke and R. J. M. Konings, *Thermochemical Data for Reactor Materials and Fission Products*. (North-Holland, Amsterdam, 1990).
16. F. Grønvold, *J. Inorg. Nucl. Chem*. **1**:357 (1955).
17. D. G. Martin, *J. Nucl. Mater.* **152**:94 (1988).
18. P. Sindzingre and M. J. Gillan, *J. Phys.: Condens. Matter*. **2**:7033 (1990).
19. N. Galamba, C. A. Nieto de Castro, and J. F. Ely, *J. Chem. Phys*. **120**:8676 (2004).
20. B. Bernu and J. P. Hansen, *Phys. Rev. Lett*. **48**:1375 (1982).
21. C. Pierleoni, G. Ciccotti, and B. Bernu, *Europhys. Lett*. **4**:1115 (1987).
22. C. Pierleoni and G. Ciccotti, *J. Phys: Condens. Matter*. **2**:1315 (1990).
23. J. K. Fink, *J. Nucl. Mater*. **279**:1 (2000).
24. P. G. Lucuta, H. Matzke, and I. J. Hastings, *J. Nucl. Mater*. **232**:166 (1996).
25. M. Amaya, T. Kubo, and Y. Korei, *J. Nucl. Sci. Technol*. **33**:636 (1996).
26. T. G. Godfrey, W. Fulkerson, T. G. Kollie, J. P. Moore, and D. L. McElroy, *J. Am. Ceram. Soc*. **48**:297 (1965).
27. J. P. Moore and D. L. McElroy, *J. Am. Ceram. Soc*. **54**:40 (1971).
28. C. Kittel, *Introduction to Solid State Physics*, 7th ed. (Wiley, New York, 1996).
29. SCDAP/RELAP5–3D© CODE MANUAL, Vol. 4: *MATPRO – A Library of Materials Properties for Light-Water-Reactor Accident Analysis*, INEEL/EXT-02–00589, Rev. 2.2 (Oct. 2003).